Autoionization distribution of atomic high doubly excited states: A ''breathing spheres'' approach

W. Huang,[1,2] U. Eichmann,[1] and W. Sandner[1,3]
[1]*Max-Born-Institut, Rudower Chaussee 6, 12489 Berlin, Germany*
[2]*Department of Modern Applied Physics, Tsinghua University, Beijing 100084, China*
[3]*Technical University, Berlin, Hardenbergstrasse 36, 10623 Berlin, Germany*
(Received 30 April 1998; revised manuscript received 1 December 1998)

By means of a time-dependent method, we have calculated final ionic state distributions after the decay of laser-prepared atomic high doubly excited, mutually penetrating $NLnl$ states. The calculation is simplified by using two nondispersive radial wave-packet wave functions with the initial condition $\langle r_1\rangle_{NL}<\langle r_2\rangle_{nl}$ at $(t=0)$. Two decay processes have been investigated. The first is the autoionization of high doubly excited states (DES) with $N\leqslant n$. Within our model it is described by two electrons moving like two ''breathing'' charge clouds exchanging energy until one of them escapes. The second decay process is the photoionization of the inner electron ($N\geqslant 2n$ including $E_N\geqslant 0$), which leaves the final ion in a high Rydberg state. Our results are compared with data from experiments, in which DES are laser-prepared using isolated core excitation. [S1050-2947(99)00404-7]

PACS number(s): 32.80.Dz, 32.80.Fb

Laser excited low-lying autoionizing Rydberg states, characterized by one electron in a Rydberg orbit and one electron in a first excited orbit, have been studied extensively both experimentally and theoretically [1,2]. The structure and the decay dynamic of these systems can be qualitatively understood in an independent-particle picture using, e.g., perturbation theory (see, for example, [1,3,4]). The most elaborate and complete theoretical description of autoionizing Rydberg states has been achieved within the framework of the multichannel quantum defect theory [5–7] together with *R*-matrix [2,8] or hyperspherical close-coupling calculations [9].

For states where both electrons are highly excited [doubly excited states (DES)], however, the situation changes dramatically. In contrast to the case of low-lying autoionizing Rydberg states, the body of available experimental data is small. Owing to largely reduced excitation cross sections of these states, elaborate excitation and detection techniques are required. DES are typically excited using an extended version of the isolated core excitation (ICE) [10], resulting in doubly excited states, where both electrons predominantly reside in different spatial regions (intershell states) [11–14]. So far the experiments have mainly focused on the investigation of the structure of DES. The increasing importance of electron correlation can be described in terms of strong polarizing forces exerted from the ''outer'' electron onto the ''inner'' one leading to a pronounced dipole structure [15,16]. Perturbative or multichannel quantum-defect theory (MQDT) treatments are no longer suitable to obtain quantitative predictions, partly because of the enormous number of interacting channels involved in the problem and partly due to the conceptual breakdown of the MQDT. The assumption that beyond a certain radius a pure Coulomb potential prevails for one of the two electrons in the resonant states is no longer fulfilled due to the increasing importance of nonlocal two-electron interaction.

Only recently, first experiments concentrated on the autoionization decay channels of DES [17–19] and the behavior of bound or doubly excited Rydberg states in an additional laser field [20–22]. In general, a detailed description of the autoionization process beyond a qualitative one [4,6,23] is still missing.

In this paper we report a time-dependent calculation of the autoionization distribution of atomic DES that results in quantitative predictions, e.g., for the average energy and the gross final ionic state distribution, which reflect the statistical behavior of the autoionization decay of the system. The approximations used are made within a combined quantum-mechanical and classical scheme. We deal only with those DES having significant mutual overlap of the wave functions of the two electrons (mutually penetrating states).

The Hamiltonian of the DES neglecting the non-Coulombic influence of a possible extended doubly charged core can be written as (atomic units are used except in the calculated results)

$$H=H_{\rm in}+H_{\rm out}+V, \tag{1}$$

where

$$H_{\rm in}=-\frac{1}{2}\nabla_1^2-\frac{2}{r_1}, \tag{2}$$

$$H_{\rm out}=-\frac{1}{2}\nabla_2^2-\frac{1}{r_2}, \tag{3}$$

and the electronic correlation

$$V=1/r_{12}-1/r_2. \tag{4}$$

V can be expanded in terms of the spherical harmonics. By taking the zeroth-order approximation, we have

$$V\simeq V_0=1/r_>-1/r_2, \tag{5}$$

where $r_>=\max(r_1,r_2)$. V_0 is a pure penetration correlation. We note that this term is usually neglected in a perturbative description of autoionizing Rydberg states, because it is assumed that the mutual penetration of the two electrons is

negligible. This assumption does not hold for the mutually penetrating DES. The mutual penetration of the two electrons of the DES becomes more and more important with increasing excitation of the inner electron.

The calculations are focused on DES prepared through the ICE scheme, which allows a direct comparison with the experimental results. We use a product of two radial wave packets as the initial wave function, i.e.,

$$\Psi_{Ll}^{Nn}(\mathbf{r}_1,\mathbf{r}_2,t)=\psi_L^N(\mathbf{r}_1,t)\psi_l^n(\mathbf{r}_2,t) \tag{6}$$

with the *inner* wave packet

$$\psi_L^N(\mathbf{r}_1,t)=\left(\sum_i c_i^N e^{-iE_i t}\phi_{iL}(\mathbf{r}_1)\right) \tag{7}$$

and the *outer* wave packet

$$\psi_l^n(\mathbf{r}_2,t)=\left(\sum_j d_j^n e^{-iE_j(t-t_0)}\varphi_{jl}(\mathbf{r}_2)\right), \tag{8}$$

where c_i^N, d_j^n are time independent and $\langle r_1\rangle<\langle r_2\rangle$ at $t=0$. In this paper, we use capital letters N,L to label the central principal quantum number and the angular momentum quantum number of the inner wave packet and the small letters n,l to label those of the outer wave packet (with or without subscript or superscript). The Pauli exchange effect, which is not included in our model, will be discussed later. In our model we neglect the influence of the wave packet dispersion (a ''frozen-width'' wave packet). Therefore, with Eq. (5) the wave packets will propagate along the hydrogenlike radial (one-dimensional) orbits until $\langle r_1\rangle=\langle r_2\rangle$ $(=r_p^{(1)})$, where the penetration between two wave packets takes place. If $\langle r_1\rangle>\langle r_2\rangle$, the outer wave packet becomes the inner wave packet and vice versa due to the electronic correlation V [Eq. (5)]. During the process an amount of orbital energy $1/r_p^{(1)}$ is transferred between the two wave packets. This is the bound state equivalent of the well-known post-collision interaction (PCI) between isotropic charge shells in the continuum [24]. The new outer wave packet may propagate to infinity if its orbital energy is positive, and thus autoionizes. Otherwise the two wave packets will penetrate each other again until eventually one of the wave packets gains enough energy to autoionize. The orbital energies $E_{N^{(i)}}$ and $E_{n^{(i)}}$ of the new inner and outer wave packets after the ith penetration are

$$E_{N^{(i)}}=E_{n^{(i-1)}}-1/r_p^{(i)}, \tag{9}$$

$$E_{n^{(i)}}=E_{N^{(i-1)}}+1/r_p^{(i)}, \tag{10}$$

where $i\geqslant 1$, $E_{n^{(0)}}=E_n$, $E_{N^{(0)}}=E_N$, and $r_p^{(i)}$ is the radial position for the wave packets when the ith penetration takes place. The orbital energies after the final penetration are labeled by $E_{N'}$ for the remaining wave packet denoted by $N'L'$ and E_k for the escaped wave packet, respectively. In our calculation the initial orbital energy $E_n<0$, but E_N can be negative or positive as shown in the following discussions.

In a dynamic picture of the autoionization process the two electrons can be regarded as two ''breathing'' charge clouds (which are isotropic in the approximation) penetrating each other and, thus, exchanging energy until one of them expands to infinity. The approximation implies no angular momentum and momentum transfers between the two wave packets. Those effects could be included by incorporating higher multipole orders. So far, the angular momentum only enters through the centrifugal part of the radial potential.

Excitation of DES usually proceeds stepwise by exciting one electron into a Rydberg orbit (the outer electron), followed by exciting the isolated inner electron resonantly or nonresonantly to a highly excited orbit, either bound or unbound. The outer electron in the Rydberg orbit remains essentially a spectator during the second excitation. To describe the dynamic process after the excitation in the framework outlined above, t_0 in Eq. (8) can be set to different values. Each value represents a value of $\langle r_2\rangle$ at the beginning and therefore a specific autoionization channel. The autoionization distribution can be obtained by integrating over t_0 in Eq. (8) except those t_0's with $\langle r_1\rangle>\langle r_2\rangle$ at $t=0$ (this part is neglected in our calculation). The possible interferences among different channels are not considered here because the general statistic behaviors are concerned. The Pauli exchange effect, not included in the above discussion, is one of the sources for the possible interferences. However, there is a special case when the effect can be neglected, i.e., when the inner electron is photoionized. This case is one of the two typical decay processes that we will discuss in the following.

In our calculation we do not follow the quantum-mechanical time-dependent approach as has been done for lower doubly excited states [25]. Instead, we substitute the radial wave packets with their classical counterparts, and the influence of the finite distribution of a wave packet over the quantum eigenstates is not taken into account in our calculation. The radial equation of motion for the particles can be written as

$$\dot{r}_j^2=2E_j+2Z_j/r_j-l_j(l_j+1)/r_j^2, \tag{11}$$

where j represents the inner or outer particle; $r_{\text{outer}}(t)>r_{\text{inner}}(t)>0$; $Z_{\text{inner}}=2$, $Z_{\text{outer}}=1$; l_j is the angular momentum; E_j is the orbital energy. It should be noted that Eq. (11) must be reconstructed after each penetration by varying E_j according to Eqs. (9) and (10), and exchanging the values of l_{inner} and l_{outer}. The treatment not only simplifies the calculation, but also makes it easier to scale the results with L/n, l/n, and E_N/E_n.

Figure 1 shows the calculated distributions among the final ionic Rydberg states $N'L'$ for two different cases for $L=l=0$. In Fig. 1(a) the distributions are shown for initially prepared autoionizing states $NLnl$ with $n\geqslant N$ $(=40)$. Obviously, the relative distribution among the lower $N'L'$ states is nearly independent of n. This stems from the fact that the penetration, which causes autoionization, takes place in the inner region where the classical kinetic energies and the potentials of the two electrons are insensitive to n. The evident influence of n appears at the cutoff of the distribution at the highest N' due to the energy requirement of the autoionization.

In Fig. 1(b), final ionic state distributions are shown for initially prepared states, where $E_N\geqslant En$ $(N\geqslant 2n)$. The distributions are almost independent of N even for $E_N\geqslant 0$. In

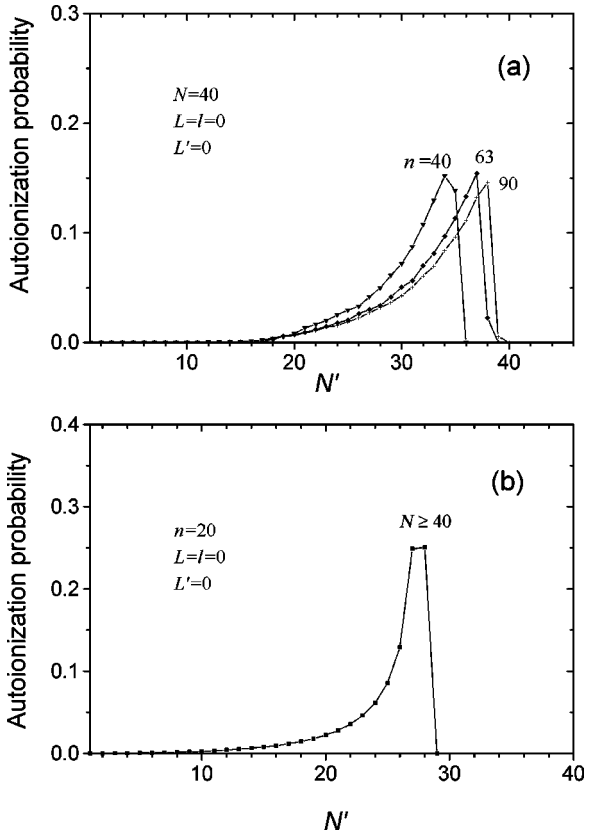

FIG. 1. Calculated distributions among the ionic Rydberg states $N'L'$ after autoionization of the DES $NLnl$ for $L=l=0$. (a) $N=40$; (b) $n=20$. Note that in (b) for $E_N \geqslant E_n$ $(N \geqslant 2n)$, the distributions are almost the same even for $E_N \geqslant 0$.

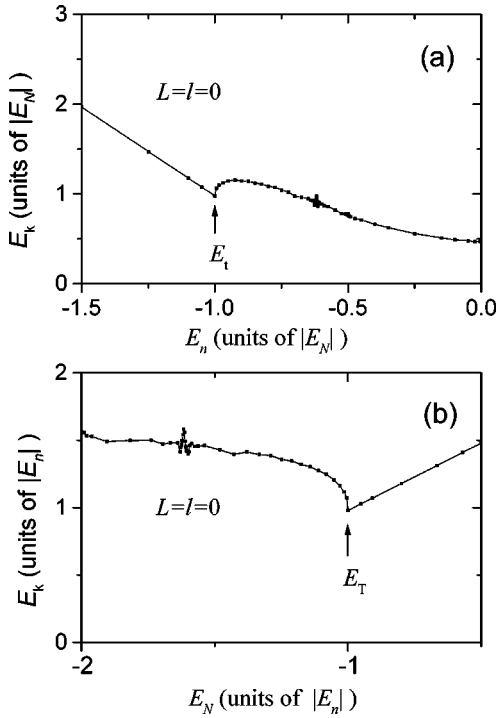

FIG. 2. Average energy of the free electron E_k after autoionization of the DES $NLnl$ $(L=l=0)$ for different E_N, E_n. The orbital energy of (a) the initial inner electron E_N (<0) is fixed; (b) the initial outer electron E_n (<0) is fixed. The fine oscillating structures at $E_n \sim 0.6E_N$ in (a) or $E_N \sim 1.6E_n$ in (b) reflect the transition processes between the autoionization process of the DES with $0 > E_n \geqslant E_N/4$ and the pure photoionization $(E_N \geqslant E_T)$ process. E_T is the threshold of E_N for pure photoionization.

this case the initial inner electron will escape after the first exchange (penetration) corresponding to the photoionization of the inner electron in a bound or lower doubly excited Rydberg state [the state before excited by the last laser photon(s)]. Photoionization is possible even for $E_N<0$ if $N \geqslant 2n$, which is different from photoinoization described in the independent-electron model. The physical scheme of this process again resembles the post-collision interaction (PCI) in Auger processes, where usually $E_N>0$ at the beginning [24]. It can be regarded as the potential exchange of the two electrons in hydrogenlike potentials. The distribution is indeed the result of the ''dynamic'' overlap of the atomic Rydberg orbit (nl) and the ionic Rydberg orbit $(N'L')$. The distribution on the energy allowed highest N''s may vanish when E_N is high enough. The energy-averaged value of N' is $1.15n$.

In the semiclassical scheme, the autoionization can be described as the penetration of the outer electron into the inner electron orbit, Fig. 1(a), and the photoionization as the penetration of the inner electron out of the outer electron orbit, Fig. 1(b).

The energy distributions of the free electron after autoionization can be easily obtained from those in Fig. 1, from which we can evaluate the average energy of the free electron E_k. Figure 2 shows the results of the DES $NLnl(L=l=0)$ for fixed E_N or E_n. For $E_N<0$, Figs. 2(a) and 2(b) are equivalent except using different units, so that $0>E_n>E_t$ in Fig. 2(a) corresponds to $E_N<E_T$ in Fig. 2(b) and $E_n<E_t$ in Fig. 2(a) corresponds to $0>E_N>E_T$ in Fig. 2(b).

In Fig. 2(a), for $n \geqslant N$ $(E_n \geqslant 0.25E_N)$, E_k varies slowly with E_n. It corresponds to the slow variation in the distribution as in Fig. 1(a) for $n \geqslant N$. In Fig. 2(b), for $N \geqslant 2n$ $(E_N \geqslant E_T = E_n)$, E_k increases in the same way as E_N increases. This means that the averaged energy transferred from the initial outer to the initial inner electron is independent of E_N (the inner will escape), and is equal to $2|E_n|$. This behavior reflects the fixed distribution in Fig. 1(b) for $N \geqslant 2n$. E_T can be regarded as the threshold of E_N for pure photoionization and is determined by the aphelion of the initial outer electron orbit. The fine oscillating structures at $E_n \sim 0.6E_N$ in Fig. 2(a) or $E_N \sim 1.6E_n$ in Fig. 2(b) reflect the transition processes between the autoionization process of the DES with $0>E_n \geqslant E_N/4$ and the pure photoionization $(E_N \geqslant E_T)$ process.

For DES with $L \neq 0$ or $l \neq 0$, the distribution and the electron average energy curves are similar to Figs. 1 and 2. The nonzero angular momentum causes the cutoff of the distribution curve at the lowest N''s due to the centrifugal potential. For $l \neq 0$, the threshold E_T in Fig. 2(b) shifts to a lower [and E_t in Fig. 2(a) to a higher] value,

$$E_t = \frac{E_N}{2}\left(1+\sqrt{1-\frac{l(l+1)}{n^2}}\right), \quad E_N<0; \tag{12}$$

$$E_T = 2E_n \Big/ \left(1+\sqrt{1-\frac{l(l+1)}{n^2}}\right), \quad E_n<0. \tag{13}$$

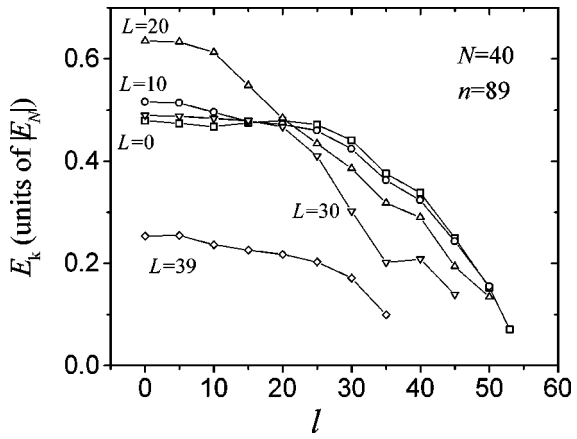

FIG. 3. Average energy of the free electron E_k after autoionization of the DES $NLnl$ ($N=40$, $n=89$) for different L,l ($E_n=0.05E_N$).

For the highest $l(=n-1)$, we have $E_T \approx 2E_n$ ($N \approx \sqrt{2}n$).

Figure 3 shows the dependence of E_k on L and l for the autoionization of DES with $N=40$ and $n=89$. If $L,l \ll N$ and $N<n$, the distributions of N' show only subtle differences when L or/and l are slightly changed. For $L \neq l$, L' may have two values L and l that indicate the escape probabilities of the initial outer electron nl and the initial inner electron NL, respectively.

For states with the same L,l and total energy (E_N+E_n), the distributions are nearly the same for different N,n if $n>N$.

In the case of pure photoionization, E_k does not depend on L and l, i.e., $E_k=E_N-2E_n$.

The calculated results show good agreement with the experimental results. For autoionization of DES $NLnl(N<n)$ in calcium, the calculation gives $N'_{\mathrm{aver}}=0.82N$ compared to $\sim 0.77N$ obtained in the experiment [18]. For photoionization of the inner electron in $5fnl$ states in strontium, the calculation gives $N'_{\mathrm{aver}}=1.15n$ compared to $\sim n$ in the experiment [20]. Here N'_{aver} is the value averaged over energy. In another experiment where the inner electron in $6snl$ states in barium is photoionized using a strong laser field [21], the highest detected final ionic state is $N'_H \approx 1.32n$ in good agreement with our calculated value $N'_H=1.41n$. It is interesting that for the photoionization of the inner electron, the final ionic state distribution of our ''dynamic'' overlap is coincidentally almost the same as that of the ''static'' overlap obtained in the ''sudden'' approximation model where the inner electron is assumed to be removed instantaneously without influencing the wave function of the outer electron. Thus it can be understood why the same N'_H is obtained in [21].

We note that there are still some discrepancies between the calculated and measured distributions. The calculated distributions are narrower than the measured ones. Furthermore, the measured distributions are shifted towards lower energies as a whole, compared to the calculated distributions. The discrepancies may arise from two aspects. One may be the neglect of higher-order terms in the expansion of the electronic correlation in our calculation, which are known to be the reason for the energy shift and distribution broadening in PCI [26]. The terms may cause the angular momentum and the momentum transfers between the wave packets and the double escape for $E_N+E_n>0$. Calculations including the terms show evidence of better agreement for the photoionization process [20]. Furthermore, we note that up to now the measured distributions rely on the saddle point model of the field-ionization method. Possible influences of magnetic quantum number m neglected in the measurements might cause the measured N' slightly lower than the actual N'. For high L or high l states [20], the effect may become more important. Electron spectroscopy [17] may avoid the difficulty.

One additional influence arises from the dispersion of the wave packets, especially for $N \ll n$, where the wave packet Eq. (7) will almost lose the localized property when the penetration takes place. In that case a form of the inner wave packet like Eq. (8) can be used. But the final distribution is almost the same as the above result.

In conclusion, we have studied the dynamic decay process in atomic DES via a time-dependent, ''breathing spheres'' approach. The method aims to interpret the statistical character of the final ionic state population. It may also be applied to slow electron collisions with Rydberg ions, ionic DES, as well as other multiple excitation processes, especially those exposed to ultrashort laser pulse.

The authors acknowledge fruitful discussions with J. Z. Tang. W.H. acknowledges support from the Alexander von Humboldt Foundation and also partial support from the National Natural Sciences Foundation of China. This work was supported by the Deutsche Forschungsgemeinschaft.

[1] T. F. Gallagher, *Rydberg Atoms* (Cambridge, New York, 1994), and references therein.
[2] M. Aymar, C.H. Greene, and E. Luc-Koenig, Rev. Mod. Phys. **68**, 1015 (1996), and references therein.
[3] P. Camus, J.-M. Lecomte, C.R. Mahon, P. Pillet, and L. Pruvost, J. Phys. II **2**, 715 (1992).
[4] S.I. Nikitin and V.N. Ostrovsky, J. Phys. B **13**, 1961 (1980).
[5] M.J. Seaton, Rep. Prog. Phys. **46**, 167 (1983).
[6] U. Fano, Rep. Prog. Phys. **46**, 97 (1983).
[7] W. Huang, Y. Zou, X.M. Tong, and J.M. Li, Phys. Rev. A **52**, 2770 (1995).
[8] Y. Komninos and C.A. Nicolaides, Phys. Rev. A **34**, 1995 (1986).
[9] A. Menzel, S.P. Frigo, S.B. Whitfield, C.D. Caldwell, M.O. Krause, J.Z. Tang, and I. Shimamura, Phys. Rev. Lett. **75**, 1479 (1995).
[10] W.E. Cooke, T.F. Gallagher, S.A. Edelstein, and R.M. Hill, Phys. Rev. Lett. **40**, 178 (1978).
[11] P. Camus, T.F. Gallagher, J.-M. Lecomte, P. Pillet, L. Pruvost, and J. Boulmer, Phys. Rev. Lett. **62**, 2365 (1989).
[12] U. Eichmann, V. Lange, and W. Sandner, Phys. Rev. Lett. **64**, 274 (1990).

[13] R.R. Jones and T.F. Gallagher, Phys. Rev. A **42**, 2655 (1990).
[14] W. Huang, X.Y. Xu, C.B. Xu, M. Xue, L.Q. Li, and D.Y. Chen, Phys. Rev. A **49**, R653 (1994).
[15] U. Eichmann, V. Lange, and W. Sandner, Phys. Rev. Lett. **68**, 21 (1992).
[16] K.-D. Heber, M. Seng, M. Halka, U. Eichmann, and W. Sandner, Phys. Rev. A **56**, 1255 (1997).
[17] M. Seng, M. Halka, K.-D. Heber, and W. Sandner, Phys. Rev. Lett. **74**, 3344 (1995).
[18] W. Huang, X.Y. Xu, C.B. Xu, P. Xue, M. Xue, and D.Y. Chen, Phys. Rev. A **54**, 5423 (1996).
[19] R. van Leeuwen, W. Ubachs, P. Camus, and W. Hogervorst, Phys. Rev. A **54**, R17 (1996).
[20] U. Eichmann, M. Seng, C. Rosen, and W. Sandner, *Laser Spectroscopy* (World Scientific, Singapore, 1998), p. 393.
[21] H. Stapelfeldt, D.G. Papaioannou, L.D. Noordam, and T.F. Gallagher, Phys. Rev. Lett. **67**, 3223 (1991).
[22] R.B. Vrijen and L.D. Noordam, J. Opt. Soc. Am. B **13**, 189 (1996).
[23] P. Rehmus and R.S. Berry, Phys. Rev. A **23**, 416 (1981).
[24] A. Niehaus, J. Phys. B **10**, 1845 (1977).
[25] W. Ihra, M. Draeger, G. Handke, and H. Friedrich, Phys. Rev. A **52**, 3752 (1995).
[26] P. van der Straten, R. Morgenstern, and A. Niehaus, Z. Phys. D **8**, 35 (1988).